Cramer-Rao Lower Bounds of Angle-of-Arrival Estimates for Acoustic Sensor Arrays Operating in Atmospheric Turbulence

S. L. Collier and D. K. Wilson
U.S. Army Research Laboratory, ATTN: AMSRL-CI-EP,
2800 Powder Mill Road, Adelphi, MD 20783-1197
301–394–2641, scollier@arl.army.mil

October 2001

Abstract

Acoustic sensor arrays will likely play a prominent role in the U. S. Army's Objective Force for applications such as target detection, identification, and location. Generally, these array systems perform direction finding by determining the wavefront angle of arrival from the phase differences across the array. However, random fluctuations in the atmosphere may strongly distort the wavefront of a sound wave. The resulting random variations in the wavefront's orientation and intensity are perceived as fluctuations in the apparent bearing angles and strength of the source. As such, the error in estimating the wavefront's angles of arrival (AOAs) will increase as the propagation distance increases and/or the strength of the turbulence increases. The Cramer-Rao lower bound (CRLB) is the statistical lower bound of the mean-square error between an estimator and its actual value. The CRLB is calculated from the probability likelihood function of the received signal. Previous formulations have modeled the probability likelihood function of a sound wave propagating through atmospheric turbulence as a zero-mean complex Gaussian distribution. The zero-mean assumption implicitly treats the case of strong scattering. In this paper the received signal is modeled as a complex Gaussian random variable with a deterministic mean, thereby generalizing the treatment to both strong and weak scattering. The CRLB of the azimuthal and elevational AOAs are calculated for both a plane-wave and a spherical-wave propagating through atmospheric turbulence with fluctuations described by a von Kármán spectrum. A single monochromatic source is considered and a line-of-sight propagation path is assumed.

Introduction

Acoustic sensor arrays have long been used in underwater applications such as target detection, identification, and location. Recently, there has been much interest within the U. S. Army to use atmospheric acoustic arrays to perform the same functions on land. Acoustical direction-finding and tracking systems will likely play a prominent role on the future battlefield, where situational awareness will be a key factor affecting the survivability of light- and medium-weight forces. Acoustic arrays are beneficial as: they are relatively inexpensive and small in size; they operate passively; obscurants, such as smoke, do not effect detection; and a line-of-sight propagation path is not necessary. Generally, these systems perform direction finding by determining the wavefront angle of arrival (AOA) from the phase differences across the array. Sound waves are strongly affected by the environment, whether it be oceanic or atmospheric. Both media are random in nature and may strongly distort the wavefront. The resulting random variations in the wavefront's orientation and intensity are perceived as fluctuations in the apparent bearing angles and strength of the source. As such, the error in estimating the wavefront's AOA will increase as the propagation distance increases and/or the intensity of the turbulence increases. (These acoustic phenomena are analogous to scintillation and quivering of optical images, as are often observed above a roadway on a sunny afternoon.) The net effects of these distortions can have a substantial impact on direction-finding in both the atmosphere [1, 2] and the ocean [3, 4].

The performance of a sensor array may be quantified by calculating the mean square error (MSE) between the estimated parameter (such as the AOA) and its actual value. The lower bound of the MSE is the Cramer-

Report Documentation Page

Report Date	Report Type	Dates Covered (from... to)
00 Oct 2001	N/A	-

Title and Subtitle Cramer-Rao Lower Bounds of Angle-of-Arrival Estimates for Acoustic Sensor Arrays Operating in Atmospheric Turbulence	**Contract Number**
	Grant Number
	Program Element Number
Author(s)	**Project Number**
	Task Number
	Work Unit Number
Performing Organization Name(s) and Address(es) U.S. Army Research Laboratory ATTN: AMSRL-CI-EP 2800 Powder Mill Road Adelphi, MD 20783-1197	**Performing Organization Report Number**
Sponsoring/Monitoring Agency Name(s) and Address(es) Department of the Army, CECOM RDEC Night Vision & Electronic Sensors Directorate AMSEL-RD-NV-D 10221 Burbeck Road Ft. Belvoir, VA 22060-5806	**Sponsor/Monitor's Acronym(s)**
	Sponsor/Monitor's Report Number(s)

Distribution/Availability Statement
Approved for public release, distribution unlimited

Supplementary Notes
See also ADM201471, Papers from the Meeting of the MSS Specialty Group on Battlefield Acoustic and Seismic Sensing, Magnetic and Electric Field Sensors (2001) Held in Applied Physics Lab, Johns Hopkins Univ, Laurel, MD on 24-26 Oct 2001. Volume 2 (Also includes 1999 and 2000 Meetings), The original document contains color images.

Abstract

Subject Terms

Report Classification unclassified	**Classification of this page** unclassified
Classification of Abstract unclassified	**Limitation of Abstract** UU

Number of Pages
20

Rao lower bound (CRLB), which is calculated from the Fisher information (FI) [5, 6]. There already exists much work in the open literature that characterizes the CRLB of array processors in the presence of noise only, (e.g., see Ottersten *et al.* [7] and the references therein). Recently, Song and Ritcey [8] developed a model that directly incorporates the effects of random media on acoustic waves into the calculation of the CRLBs of AOA estimates. Specifically, they considered propagation in an ocean channel with random inhomogeneities having a Gaussian spatial correlation. Using the general framework of Song and Ritcey, Wilson [9] calculated the performance bounds on AOA estimates using various correlation functions that are representative of atmospheric turbulence.

Song and Ritcey [8] and Wilson [9] modeled the received signal as a complex, zero-mean, Gaussian random variable. By assuming that the signal of interest had a zero-mean, they implicitly treated the case of waves strongly scattered by the turbulence. A strong scattering event occurs when the turbulence is sufficiently strong, and/or the wavefronts propagate a sufficient distance, so that the phase of the received signal at each sensor is completely randomized. However, in many practical problems the variance of the index-of-refraction fluctuations is sufficiently small, or the propagation distance is sufficiently short, that the waves have only been weakly scattered when they arrive at the array. A weakly scattered wave has a mean component significantly larger than the standard deviation of the real and imaginary parts of the signal.

Moreover, in the previous work of Wilson [9], the FI was calculated assuming that the only unknown was the wavefront AOA (azimuth only). The source-receiver propagation distance, turbulence parameters, and signal-to-noise ratio (SNR) were implicitly assumed to be known. In a real scenario, this information may not be available. A more relevant analysis would therefore use a multivariate formalism.

This paper provides an analysis of the CRLBs of AOA estimates for a passive sensor array operating in a turbulent medium. The zero-mean assumption is avoided, so that the model is valid for both strong and weak scattering. To capture scattering by eddies in both the energy-containing and inertial subranges, a von Kármán spectrum is used for the turbulence [10]. Furthermore, the analysis from Ref. [9] is expanded to include the propagation distance, SNR, turbulence parameters, and phase of the source in the unknown parameter set. The extent to which the estimates of the AOAs will degrade when they are simultaneously estimated with other parameters is determined by calculating the coupling between the estimates.[1]

Three-dimensional (3D) propagation is considered for an incident plane wave and spherical wave. For simplicity a single monochromatic source and a line-of-sight propagation path are assumed. A brief review of the phenomology of atmospheric turbulence is given in Section 1. The theoretical model is developed in Section 2 and the Cramer-Rao lower bound is formulated in Section 3. Results are given in Section 4 and conclusions are drawn in Section 5.

1 Phenomenology

The atmospheric boundary layer generally refers to the layer of air directly above the earth's surface in which effects, such as heating, cooling, and friction, are felt on a short time scale (less than a day). This layer is usually one-half a kilometer to several kilometers thick. Fluctuations in momentum, heat, or matter may result in turbulent motions that have scales on the order of the depth of the boundary layer or less. Some characteristics of turbulent flows are: they have purely rotational motion; they are three-dimensional; and they are dissipative and thus require energy to be sustained. When a tangential force exists at a boundary, a shear turbulence occurs. Buoyant turbulent motion may result, e.g., from the thermal heating of the ground which induces an upward motion of the air. Turbulent motion may be characterized by an inner scale length and an outer scale length ($\mathcal{L}$). In between the inner and outer scales lies the inertial subrange, characterized by a cascade of energy to progressively smaller scales. (See, e.g., Reference [11].)

[1]The theoretical treatment in this paper applies to the AOAs, which represent the orientation of the wavefront normal when the sound reaches the array. For propagation in the atmosphere, the average horizontal (azimuthal) AOA is usually very close to the actual angle of bearing (AOB) of the source, thereby making acoustic arrays well suited to determining the horizontal position of a source. However, for the vertical (elevational) AOA, the situation is quite different. Atmospheric refraction may bend the soundwaves upward or downward, thus interfering with the ability to determine the AOB. As such, most existing acoustic ground sensors do not attempt to determine the elevation of a near-ground source.

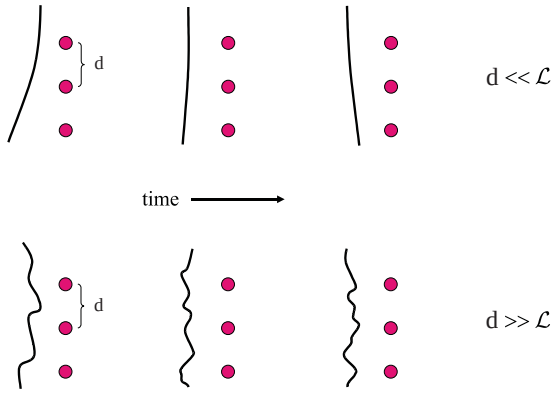

Figure 1: Turbulence-induced distortion of acoustic wavefronts impinging on a sensor array.

As an acoustic wavefront propagates from the source to the sensor array, it is distorted by random fluctuations in the atmosphere. A coherence loss results when the phase and amplitude relationship between the sensors becomes random. Let the separation between the sensors be d, and let $\mathcal{L}$ be the characteristic length of the largest turbulent eddies. For $d \ll \mathcal{L}$ the wavefronts will be smooth and nearly planar when arriving at the sensor array. But if $d \gg \mathcal{L}$, the wavefronts will have a rough and random appearance when observed on the scale of the array. These cases are depicted in Fig. 1. In both cases, there is a coherence loss between the sensor signals.

Knowing $\mathcal{L}$ is essential to designing a sensor array. Typical values of $\mathcal{L}$ during the daytime range between 50 m (for strong winds and little solar heating of ground) and 500 m (for sunny afternoons with light winds). Most sensor arrays employed by the Army have an aperature of about 1 m. Therefore, the case $d \ll \mathcal{L}$ generally applies. It is also generally desirable to space array elements less than one-half a wavelength apart to prevent spurious source images (e.g., spatial aliasing effects).

2 Theoretical Model

Calculation of the FI requires a priori knowledge of the probability density function (PDF) of the received signal. In this section a theoretical model that incorporates the effects of turbulence on the source signal is developed to describe the PDF of the received signal. Let us define the notation that shall be used throughout this paper: $[\cdot]^*$ denotes the complex conjugate, $[\cdot]^{\mathrm{T}}$ the transpose, $[\cdot]^\dagger$ the Hermitian adjoint (complex conjugate transpose), and $\langle\cdot\rangle$ the ensemble average.

Consider an acoustic array with N sensors. We assume that the signal at each sensor results from: (1) the wave that has propagated from the source of interest with ϕ and θ as the azimuthal and elevational angles of arrival, respectively, and (2) random noise. Let $\mathbf{p}(\phi, \theta, t)$ and $\mathbf{n}(t)$ be the time-varying complex envelops of the two contributions, respectively. These column vectors have N elements, one element corresponding to each sensor. The source contribution is time dependent because of the random turbulent effects. The noise, which is also time dependent, may result from wind noise or other competing sources. The total received signal is

$$\mathbf{s}(\phi, \theta, t) = \mathbf{p}(\phi, \theta, t) + \mathbf{n}(t)\,. \tag{1}$$

Let us assume that the source and the noise signals are uncorrelated and that the noise signals at the sensors are mutually uncorrelated with equal variance. Let us further assume that the noise component has a Gaussian distribution with a zero mean and variance σ_n^2. Although exact solutions for the pressure field of the source and its PDF are unknown, solutions to its first and second moments can be found in the literature. We therefore approximate that $\mathbf{p}$ has a Gaussian distribution with mean $\boldsymbol{\mu}$ and covariance matrix $\mathbf{C}_p$, whose elements are

$$\mu_i = \langle p_i \rangle \qquad \text{and} \qquad [\mathbf{C}_p]_{ij} = \left\langle p_i p_j^* \right\rangle - \mu_i \mu_j^*\,. \tag{2}$$

We use the results in the open literature for acoustic wave propagation in a random medium to determine μ_i and $\langle p_i p_j^* \rangle$ as discussed in the following section. The total signal $\mathbf{s}$ is thus Gaussian distributed with mean $\boldsymbol{\mu}$ and covariance

$$\mathbf{C} = \mathbf{C}_p + \sigma_n^2 \mathbf{I}_N. \tag{3}$$

This signal model, in which the real and imaginary parts are modeled as Gaussian random variables with equal variances, is reasonable for strong scattering, or for weak scattering, in the presence of strong diffraction (the Rytov extension region). It is less well suited to situations where both scattering and diffraction are weak (geometric acoustics), in which case the phase variance dominates the signal behavior [12].

2.1 First and Second Moments: Normal Incidence

The pressure field associated with a sound wave propagating in a moving medium is characterized by a closed set of fluid dynamic equations. The small angle parabolic equation method may be used to reduce this set of equations to a single wave equation. The Markov approximation, which assumes that the turbulence field has vanishing correlation in the direction of propagation, may then be used to obtain the statistical moments of the sound field in closed form. These approximations are valid in far field, for small scattering angles, and for $\mathcal{L} \gg \lambda > \ell$, where λ is the wavelength, and $\mathcal{L}$ and ℓ are, respectively, the outer (integral) and inner (Kolmogorov) length scales of the turbulence. We use the solution for the first and second moments of the pressure field as given by Ostashev [10], who generalized the results of [13] and [14] to include fluctuations in the medium velocity. The solution for the second moment is, however, strictly valid for normal incidence across two sensors. These results are outlined in the following paragraphs.

By using the small angle parabolic and Markov approximations, one finds that the first and second moments of the pressure field undergo an exponential attenuation. Consider a sound wave that is propagating along the x-axis with wave number $\mathbf{k}$, $k = 2\pi/\lambda$. Let $\mathbf{r} = [x,\ y,\ z]$ be the observation point and $\mathbf{r}^\perp = [0,\ y,\ z]$ be its component transverse to $\mathbf{k}$. For $x \gg r^\perp$, the first moment at $\mathbf{r}$ is

$$\left\langle\ p(\mathbf{r})\ \right\rangle = p_{\text{H}}\left(\mathbf{r}\right)\ e^{-\gamma x}\,, \tag{4}$$

where γ is the extinction coefficient for the first moment and $p_{\text{H}}(\mathbf{r})$ is the sound pressure field in the absence of random inhomogeneities. For a plane wave

$$p_{\text{H}}(\mathbf{r}) = p_0\, e^{\mathrm{i}(\mathbf{k}\cdot\mathbf{r}+\chi)}\,, \tag{5}$$

where p_0 is the pressure amplitude (a real-valued constant) and χ is the phase of the source. Here the propagation is strictly along the x-axis, therefore $p_{\text{H}}(\mathbf{r}) = p_0\, e^{\mathrm{i}(kx+\chi)}$. For a spherical wave

$$p_{\text{H}}(\mathbf{r}) = p_0\, e^{\mathrm{i}(kr+\chi)}\,, \quad \text{where} \quad p_0 = \frac{\mathcal{A} r_0}{r}\,, \tag{6}$$

and where $\mathcal{A}$ is the pressure at $r = r_0$ ($\mathcal{A}$ and r_0 are real-valued constants). The parabolic approximation for a spherical wave propagating in free space (used in the solution to the wave equation) is

$$\frac{\exp\left(\mathrm{i}kr\right)}{r} \approx \frac{1}{x}\exp\left(\mathrm{i}kx\right)\exp\left(\mathrm{i}\frac{k{r^\perp}^2}{2x}\right)\,. \tag{7}$$

It is the first order approximation in $r^\perp/x$.

The first moment represents the unscattered (deterministic) part of the wavefield. We define the saturation parameter parameter Ω as

$$\Omega = 1 - e^{-2\gamma x}\,. \tag{8}$$

When $\gamma x \ll 1$, the saturation parameter is close to 0, scattering is small, and the signal at a single sensor exhibits little variability. When $\gamma x \gg 1$, $\Omega \approx 1$, and the scattered part of the field dominates.

Consider now two points near the x-axis, $\mathbf{r}_1 = [x,\ y_1,\ z_1]$ and $\mathbf{r}_2 = [x,\ y_2,\ z_2]$, where $x \gg r_1^\perp,\ r_2^\perp$. The second moment is

$$\left\langle\ p\left(\mathbf{r}_1\right)\ p^*\left(\mathbf{r}_2\right)\ \right\rangle = p_{\text{H}}\left(\mathbf{r}_1\right)\ p_{\text{H}}^*\left(\mathbf{r}_2\right)\ e^{-\alpha(\rho)x}\,, \tag{9}$$

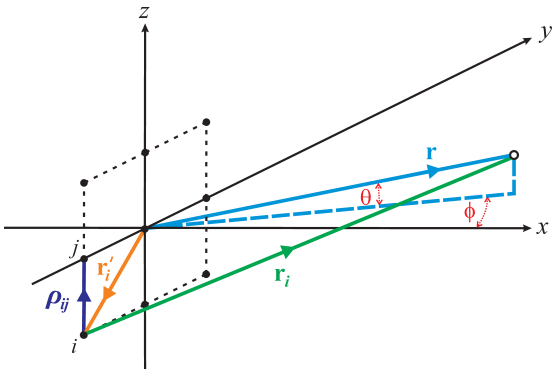

Figure 2: Coordinate system. The closed circles represent the sensors. For a plane wave, the open circle represents the point in the plane of the source at which $\mathbf{r}$ is normal to the wavefront. For a spherical wave, the open circle represents the source. The azimuthal and elevational AOAs, ϕ and θ, are defined with respect to $\hat{\mathbf{r}}$.

where $\boldsymbol{\rho} = \mathbf{r}_1 - \mathbf{r}_2$ is the sensor separation vector (transverse to the propagation direction), α is the extinction coefficient for the second moment, and $p_{\text{H}}(\mathbf{r}_i)$ is given by Eq. (5) for a plane wave and Eq. (6) for a spherical wave. [Again the parabolic approximation for a spherical wave propagating in free space, Eq. (7), was used to obtain this result. It is, however, more convenient to use the expression in Eq. (6). Provided we stay within the constraints of the approximation, it does not matter which expression we use.] The extinction coefficients for the first and second moments are related by

$$\gamma = \alpha(\infty)/2\,. \tag{10}$$

2.2 First and Second Moments: Oblique Incidence

We now wish to derive expressions for the first and second moments for nominally oblique incidence. Consider a sound wave that is propagating with wave number $\mathbf{k}$, where $\mathbf{k}$ is no longer parallel to the x-axis. Let $[\cdot]^{\perp}$ and $[\cdot]^{\parallel}$ denote the components of a vector transverse and parallel to $\hat{\mathbf{k}}$, respectively. For both a plane wave and a spherical wave, r is the propagation distance of the wavefront to the center of the array. However, the definition of the vector $\mathbf{r}$ depends upon the case considered: for a plane wave, $\mathbf{r}$ is the vector from the center of the array normal to the plane of the source; for a spherical wave, $\mathbf{r}$ is the vector from the center of the array to the source. A list of vectors and their definitions is given in Table 1. For both a plane wave and a spherical wave, the azimuthal and elevational AOAs, ϕ and θ, are measured with respect to the center of the array, so that $\hat{\mathbf{r}} = [\cos\phi\cos\theta,\ \sin\phi\cos\theta,\ \sin\theta]^{\mathrm{T}}$. An illustration is given in Fig. 2.

For this analysis we take the first moment at the ith sensor to be

$$\text{Plane Wave}: \qquad \mu_i \approx p_0 e^{\mathrm{i}(\mathbf{k}\cdot\mathbf{r}_i+\chi)} e^{-\gamma r}\,, \qquad p_0 = \text{constant} \tag{11}$$

$$\text{Spherical Wave}: \qquad \mu_i = p_0 e^{\mathrm{i}(kr_i+\chi)} e^{-\gamma r}\,, \qquad p_0 \approx \frac{\mathcal{A} r_0}{r}\,. \tag{12}$$

For both the plane wave and spherical wave, the phase of the first moment is not modified, but the magnitude of each is. In other words, we assume that the largest source of variation of the first moment between the center of the array and the ith sensor is due to the phase not the attenuation. These approximations are valid provided that for every i and j

$$\text{Plane Wave}: \qquad e^{-\gamma r_i^{\parallel}} \approx e^{-\gamma r_j^{\parallel}} \approx e^{-\gamma r} \tag{13}$$

$$\text{Spherical Wave}: \qquad \frac{e^{-\gamma r_i}}{r_i} \approx \frac{e^{-\gamma r_j}}{r_j} \approx \frac{e^{-\gamma r}}{r}\,. \tag{14}$$

It follows that the saturation parameter, for both a plane wave and a spherical wave, is now

$$\Omega \approx 1 - e^{-2\gamma r}\,. \tag{15}$$

	Plane Wave	**Spherical Wave**
$\mathbf{r} = [x,\ y,\ z]^{\mathrm{T}}$	Vector from the center of the array normal to the plane of the source	Vector from the center of array to the source
$x = \cos\phi\cos\theta$ $y = \sin\phi\cos\theta$ $z = \sin\theta$	Components of $\mathbf{r}$ in terms of the azimuthal and elevational angles of arrival ϕ and θ	
$r = \lvert\mathbf{r}\rvert$	Propagation distance of the wavefront to the center of the array	
$\hat{\mathbf{r}} = \mathbf{r}/r$	Unit vector in direction of $\mathbf{r}$	
$\hat{\mathbf{e}}_r$	N/A	Radial orthogonal unit vector in spherical coordinates
$\mathbf{k}$	Wave number. $\lvert\mathbf{k}\rvert = k = 2\pi/\lambda$, where λ is the wavelength	
	$\mathbf{k} = -k\hat{\mathbf{r}}$	$\mathbf{k} = k\hat{\mathbf{e}}_r$
$\mathbf{r}'_i = [x'_i,\ y'_i,\ z'_i]^{\mathrm{T}}$	Vector from the center of the array to the ith sensor	
$\mathbf{r}_i = \mathbf{r} + \mathbf{r}'_i$	As defined	Vector from the source to the ith sensor
$r_i = \lvert\mathbf{r}_i\rvert$	As defined	Propagation distance of the wavefront to the ith sensor
$r_i^{\parallel} = \lvert\mathbf{r}_i \cdot \hat{\mathbf{k}}\rvert$	Propagation distance of the wavefront to the ith sensor	$r_i^{\parallel} = r_i$
$r_i^{\perp} = \lvert\mathbf{r}_i \times \hat{\mathbf{k}}\rvert$	Magnitude of the component of $\mathbf{r}_i$ that is transverse to direction of wave propagation	$r_i^{\perp} = 0$
$\boldsymbol{\rho}_{ij} = \mathbf{r}'_i - \mathbf{r}'_j$	Vector between the ith and jth sensors	
$\rho_{ij} = \lvert\boldsymbol{\rho}_{ij}\rvert$	Distance between the ith and jth sensors	
$\rho_{ij}^{\perp} = \lvert\boldsymbol{\rho}_{ij} \times \hat{\mathbf{k}}\rvert$	Magnitude of the component of $\boldsymbol{\rho}_{ij}$ that is transverse to the direction of wave propagation	

Table 1: Definitions of vectors and their magnitudes. Physical descriptions are provided when possible. Refer to Fig. 2.

Strictly speaking, Eq. (9) for the second moment is valid for normal incidence across sensors i and j, i.e., when $r_i^{\parallel} = r_j^{\parallel}$ and hence and hence $\boldsymbol{\rho}_{ij}^{\perp} = \boldsymbol{\rho}_{ij}$. For oblique incidence we approximate

$$\text{Plane Wave}: \qquad \left\langle p_i p_j^* \right\rangle \approx p_0^2 e^{\mathrm{i}\mathbf{k}\cdot(\mathbf{r}_i - \mathbf{r}_j)} e^{-\alpha(\rho_{ij})\, r}\,, \qquad p_0 = \text{constant} \tag{16}$$

$$\text{Spherical Wave}: \qquad \left\langle p_i p_j^* \right\rangle \approx p_0^2 e^{\mathrm{i}k(r_i - r_j)} e^{-\alpha(\rho_{ij})\, r}\,, \qquad p_0 \approx \frac{\mathcal{A} r_0}{r}\,. \tag{17}$$

We are thereby assuming that for every i and j,

$$\alpha\left(\rho_{ij}^{\perp}\right) \approx \alpha\left(\rho_{ij}\right) \tag{18}$$

and

$$\text{Plane Wave :} \qquad e^{-\alpha(\rho_{ij})r_i^{\parallel}} \approx e^{-\alpha(\rho_{ij})r_j^{\parallel}} \approx e^{-\alpha(\rho_{ij})r} \tag{19}$$

$$\text{Spherical Wave :} \qquad \frac{e^{-\alpha(\rho_{ij})r_i}}{r_i r_j} \approx \frac{e^{-\alpha(\rho_{ij})r_j}}{r_i r_j} \approx \frac{e^{-\alpha(\rho_{ij})r}}{r^2}\,. \tag{20}$$

A careful and consistent treatment of the magnitudes of the moments is necessary to ensure a nonsingular covariance matrix. The phases of the first and second moments must also be treated consistently to ensure that the covariance matrix is nonsingular. Because of these approximations, we restrict our investigation to nominally normal incidence to a planar array for 3D propagation [a linear array for two-dimensional (2D) propagation].

2.3 Covariance Matrix and Mean

We write the first and second moments in the form

$$\mu_i = \tilde{\mu} e^{\mathrm{i}\Phi_i} \qquad \text{and} \qquad \left\langle\, p_i p_j^* \,\right\rangle = p_0^2 e^{-\alpha(\rho_{ij})\,r} e^{\mathrm{i}\Phi_{ij}}\,, \tag{21}$$

where we define[2]

$$\tilde{\mu} = p_0 e^{-\gamma r} \qquad \text{and} \qquad \Phi_{ij} = \Phi_i - \Phi_j\,. \tag{22}$$

For a plane wave p_0 is as defined in Eq. (5) and

$$\Phi_i = \mathbf{k}\cdot\mathbf{r}_i + \chi = k\left(r + x_i'\cos\phi\cos\theta + y_i'\sin\phi\cos\theta + z_i'\sin\theta\right) + \chi\,; \tag{23}$$

and for a spherical wave p_0 is as defined in Eq. (12) and

$$\Phi_i = kr_i + \chi = k\left[r^2 + r_i'^2 + 2r\left(x_i'\cos\phi\cos\theta + y_i'\sin\phi\cos\theta + z_i'\sin\theta\right)\right]^{1/2} + \chi\,. \tag{24}$$

Thus the elements of the total covariance matrix [Eq. (3)] are

$$C_{ii} = p_0^2 - \tilde{\mu}^2 + \sigma_n^2 \qquad \text{and} \qquad C_{ij} = \left[p_0^2\, e^{-\alpha(\rho_{ij})\,r} - \tilde{\mu}^2\right] e^{\mathrm{i}\Phi_{ij}}\,,\ i \neq j\,. \tag{25}$$

The mutual coherence function (MCF) between the ith and jth sensors is defined to be the positive square root of

$$\Gamma_{ij}^2 = \frac{\left\langle p_i p_j^* \right\rangle \left\langle p_i^* p_j \right\rangle}{\left\langle p_i p_i^* \right\rangle \left\langle p_j p_j^* \right\rangle}\,. \tag{26}$$

Thus for both the plane-wave and spherical-wave treatments here,

$$\Gamma_{ij} = |\left\langle p_i p_j^* \right\rangle| / p_0^2 = e^{-\alpha(\rho_{ij})\,r}. \tag{27}$$

The minimum value of the MCF for $\rho_{ij} \to \infty$ is $\Gamma_{\min} = e^{-2\gamma r}$.

An advantage to this formulation of the first and second moments for the plane-wave treatment is that the resulting covariance matrix $\mathbf{C}_p$ and mean $\boldsymbol{\mu}$ may be written in terms of the MCF matrix $\boldsymbol{\Gamma}$, a steering vector $\boldsymbol{\mathcal{s}}$, and a steering matrix $\boldsymbol{\mathcal{S}}$. The steering vector is defined to be

$$\boldsymbol{\mathcal{s}} = \left[e^{\mathrm{i}\mathbf{k}\cdot\mathbf{r}_1},\ e^{\mathrm{i}\mathbf{k}\cdot\mathbf{r}_2},\ \cdots,\ e^{\mathrm{i}\mathbf{k}\cdot\mathbf{r}_N}\right]^{\mathrm{T}}\,. \tag{28}$$

The steering matrix represents the phase delay between the sensors due solely to the difference in propagation length. As $\boldsymbol{\mathcal{S}} = \boldsymbol{\mathcal{s}} \otimes \boldsymbol{\mathcal{s}}^{\dagger}$, where $\otimes$ is the (right) Kronecker product,

$$\mathcal{S}_{ij} = \exp\left(\mathrm{i}\mathbf{k}\cdot\boldsymbol{\rho}_{ij}\right). \tag{29}$$

[2]Note that we use the convention that μ_i is the ith component of the vector $\boldsymbol{\mu}$, (i.e., the value of the first moment of the sound field at the ith sensor), and is given by $\mu_i = \tilde{\mu} e^{\mathrm{i}\Phi_i}$. In this manner, $|\mu_i| = \tilde{\mu}$ and $|\boldsymbol{\mu}| = \mu = \sqrt{n}\tilde{\mu}$.

Therefore for an incident plane wave

$$\boldsymbol{\mu} = p_0 \Gamma_{\min}^{1/2}\, \boldsymbol{s} \qquad \text{and} \qquad \mathbf{C}_p = p_0^2 \boldsymbol{\Gamma} \odot \boldsymbol{\mathcal{S}} - p_0^2 \Gamma_{\min} \boldsymbol{\mathcal{S}}\,, \tag{30}$$

where $\odot$ is the Hadamard product (element-by-element multiplication).

We may also write the moments for a spherical wave in the same form as Eq. (30), but $\boldsymbol{s}$ and $\boldsymbol{\mathcal{S}}$ are defined from the phases:

$$\boldsymbol{s} = \left[e^{\mathrm{i}kr_1},\ e^{\mathrm{i}kr_2},\ \cdots,\ e^{\mathrm{i}kr_N}\right]^{\mathrm{T}} \qquad \text{and} \qquad \boldsymbol{\mathcal{S}} = \boldsymbol{s} \otimes \boldsymbol{s}^{\dagger} \rightarrow \mathcal{S}_{ij} = \exp\left[\mathrm{i}k\left(r_i - r_j\right)\right]\,. \tag{31}$$

Though the meaning of a steering vector and array is lost, these mathematical expressions may be useful for computational purposes.

2.4 von Kármán Turbulence Model

The extinction coefficients depend on the structure of the random medium. For a plane wave

$$\alpha(\rho) = 2\pi k^2 \left[f(0) - f(\rho)\right]\,, \tag{32}$$

and for a spherical wave

$$\alpha(\rho) = 2\pi k^2 \int_0^1 \left[f(0) - f(\rho u)\right] du\,, \tag{33}$$

where f is the 2D (or projected) correlation function for the sound-speed fluctuations [10, 15, 16, 17]. For most random media, including a turbulent atmosphere, $\alpha(\rho)$ initially increases monotonically with increasing ρ, but when ρ exceeds $\mathcal{L}$, $\alpha(\rho)$ asymptotically approaches a constant value [15]. Since $f(\rho) \rightarrow 0$ in the limit $\rho \rightarrow \infty$, this constant value is simply 2γ, given by

$$2\gamma = 2\pi k^2 f(0) = 2\varsigma^2 k^2 \mathcal{L}\,, \tag{34}$$

where ς^2 is the index-of-refraction variance. Hence the second moment will initially decrease with increasing ρ, but will eventually "saturate" at a fixed minimum value.

Typical acoustic sensor arrays employed by the Army have a sensor spacing larger than the height of the array from ground. As such, the performance of these arrays is affected by the large eddies of the energy-containing (or source) subranges of the turbulence spectrum. (By contrast, the performance of optical systems is dependent primarily upon the smaller-scale eddies in the inertial and dissipation subranges.) The isotropic, homogeneous von Kármán turbulence model describes the inertial subrange of the turbulence spectrum more realistically than the commonly used Gaussian models, and it still behaves reasonably in the energy-containing subrange. The von Kármán form for the 2D correlation function is dependent upon the source of the sound speed fluctuations: a scalar field is induced by temperature or humidity fluctuations and a vector field is induced by wind velocity fluctuations. The 2D correlation functions for a scalar field f_s and a vector field f_v, may be written in the form (see Eq. (49) in Ref. [17] and Eq. (7.112) in Ref. [10])

$$f_s(\rho, \varsigma^2, l) = \frac{2\varsigma^2 l}{\sqrt{\pi}\,\Gamma\left(1/3\right)} \left(\frac{\rho}{2l}\right)^{5/6} K_{5/6}\left(\frac{\rho}{l}\right) \tag{35}$$

$$f_v(\rho, \varsigma^2, l) = \frac{2\varsigma^2 l}{\sqrt{\pi}\,\Gamma\left(1/3\right)} \left(\frac{\rho}{2l}\right)^{5/6} \left[K_{5/6}\left(\frac{\rho}{l}\right) - \frac{\rho}{2l} K_{1/6}\left(\frac{\rho}{l}\right)\right]\,, \tag{36}$$

where $l = \Gamma(1/3)\mathcal{L}/\left[\sqrt{\pi}\Gamma(5/6)\right]$ is a characteristic length scale, $\Gamma(x)$ is the Gamma function, and $K_\nu(x)$ is the modified Bessel function of order ν. The equation for f_s in this paper differs somewhat from that of Ref. [9] due to the manner in which the scalar energy spectrum was defined in that paper. The equation in this paper is consistent with the more standard definition found in Ref. [10].

The MCF for an incident plane wave is plotted in Fig. 3 as a function of the index-of-refraction variance ς^2 and the characterstic length scale normalized by the wavelength l/λ for both a scalar and a vector

von Kármán spectrum. In presenting the results, it is natural to use normalized length scales, (e.g., r/λ, d/λ, etc.), as then the coherence has no explicit wavelength dependence. In (a) and (b) the MCFs are calculated for $\rho/\lambda = 0.5$ and $r/\lambda = 500$. [For example, a tank has a frequency of roughly 200 Hz. Thus, as the wavelength is the average sound speed (about 340 m/s) divided by the frequency, λ is roughly 2 m. Therefore if the tank is at a range of one kilometer, $r/\lambda \sim 500$.] The coherence for both spectra decreases significantly in the regions where the index-of-refraction variance is large, $\varsigma^2 \sim 10^{-4}$, and the normalized length scale is small, $10 < l/\lambda < 1$. In (c) and (d) the same is calculated but for $\rho/\lambda = 3/\sqrt{2}$. The larger sensor separation leads to a more rapid decrease in the MCFs as functions of the turbulence parameters. For both sensor separations the MCF for the vector spectrum is more sensitive to the changes in the turbulence parameters, and its minimum with respect to the turbulence parameters (for a fixed finite sensor separation and normalized propagation distance) is smaller than that for the scalar spectrum. [We note that $\alpha(\rho_{ij})r$ is dependent upon the product of $\varsigma^2 r/\lambda$. Therefore, one may view the x-axis in Fig. 3 as a change in the product of $\varsigma^2 r/\lambda$.] In Fig. 4 the same is plotted but for an incident spherical wave. The function $\Gamma_{\min}$ (the minimum value of the MCF as a function of sensor separation ($\rho = \infty$) for fixed propagation distance and fixed turbulence parameters) is the same for both a scalar and a vector spectrum and for both a plane wave and spherical wave. It is plotted in Fig. 5. Even though its value is only dependent upon the product $\varsigma^2 rl/\lambda^2$, it is plotted versus the turbulence parameters at $r/\lambda = 500$ for ease of comparison with Figs. 3 and 4.

3 Formulation

3.1 Cramer-Rao Lower Bound

Consider the vector parameter $\mathbf{\Theta} = [\Theta_1,\ \Theta_2,\ ...,\ \Theta_{\mathcal{N}}]^{\mathrm{T}}$ that we wish to estimate. The minimum MSE of an unbiased estimator $\hat{\mathbf{\Theta}}$ about its actual value $\mathbf{\Theta}$ may be calculated from the Cramer-Rao theorem [5, 6], which gives

$$\left\langle\ (\Theta_\nu - \hat{\Theta}_\nu)^2\ \right\rangle \geq \left[\mathbf{J}^{-1}(\mathbf{\Theta})\right]_{\nu\nu}\ , \tag{37}$$

where $\mathbf{J}(\mathbf{\Theta})$ is the $\mathcal{N} \times \mathcal{N}$ FI matrix. (An estimator is said to be unbiased if and only if $\left\langle \hat{\mathbf{\Theta}} \right\rangle = \mathbf{\Theta}$.) The FI is related to the probability likelihood $\wp(\mathbf{x};\, \mathbf{\Theta})$ (PDF of $\mathbf{x}$ with $\mathbf{\Theta}$ as a parameter) by

$$\left[\mathbf{J}(\mathbf{\Theta})\right]_{\lambda\nu} = -\left\langle\ \frac{\partial^2 \ln \wp(\mathbf{x};\, \mathbf{\Theta})}{\partial\Theta_\lambda \partial\Theta_\nu}\ \right\rangle, \tag{38}$$

where the expectation value is taken with respect to $\wp(\mathbf{x};\, \mathbf{\Theta})$ and the derivatives are evaluated at the true value of $\mathbf{\Theta}$.

The likelihood function for real parameters of complex Gaussian PDF with covariance matrix $\mathbf{C}_{\mathbf{x}}(\mathbf{\Theta})$ and mean $\boldsymbol{\mu}(\mathbf{\Theta})$ may be written [5]

$$\wp(\mathbf{x};\, \mathbf{\Theta}) = \frac{1}{\pi^{\mathcal{N}} \det\left[\mathbf{C}_{\mathbf{x}}(\mathbf{\Theta})\right]} \exp\left\{ -\left[\mathbf{x} - \boldsymbol{\mu}(\mathbf{\Theta})\right]^\dagger \mathbf{C}_{\mathbf{x}}^{-1}(\mathbf{\Theta})\left[\mathbf{x} - \boldsymbol{\mu}(\mathbf{\Theta})\right] \right\}. \tag{39}$$

Its corresponding FI is [5]

$$\left[\mathbf{J}(\mathbf{\Theta})\right]_{\lambda\nu} = \mathrm{tr}\left(\mathbf{C}^{-1} \frac{\partial \mathbf{C}}{\partial\Theta_\lambda}\, \mathbf{C}^{-1}\, \frac{\partial \mathbf{C}}{\partial\Theta_\nu} \right) + 2\Re\left(\frac{\partial \boldsymbol{\mu}^\dagger}{\partial\Theta_\lambda}\, \mathbf{C}^{-1}\, \frac{\partial \boldsymbol{\mu}}{\partial\Theta_\nu} \right), \tag{40}$$

where the functional dependence has been suppressed. If there are M independent and identically distributed data sets, then the likelihood function will be the product of M identical distribution functions, and hence the FI is M times the quantity given in Eq. (40). Suppose there are N elements in the sensor array. Then $\mathbf{C}$ is an $N \times N$ matrix, and $\boldsymbol{\mu}$ is a column vector of length N. Let us use the convention that the subscripts $\lambda,\, \nu \in [1,\, \ldots,\, \mathcal{N}]$ are the indices on the parameters and that $i,\, j \in [1,\, \ldots,\, N]$ are the indices on the elements of the sensor array.

Let us define $\sigma_\nu \equiv \sqrt{\left[\mathbf{J}^{-1}\right]_{\nu\nu}}$. We loosely refer to either σ or σ^2 as the CRLB, as the meaning should be

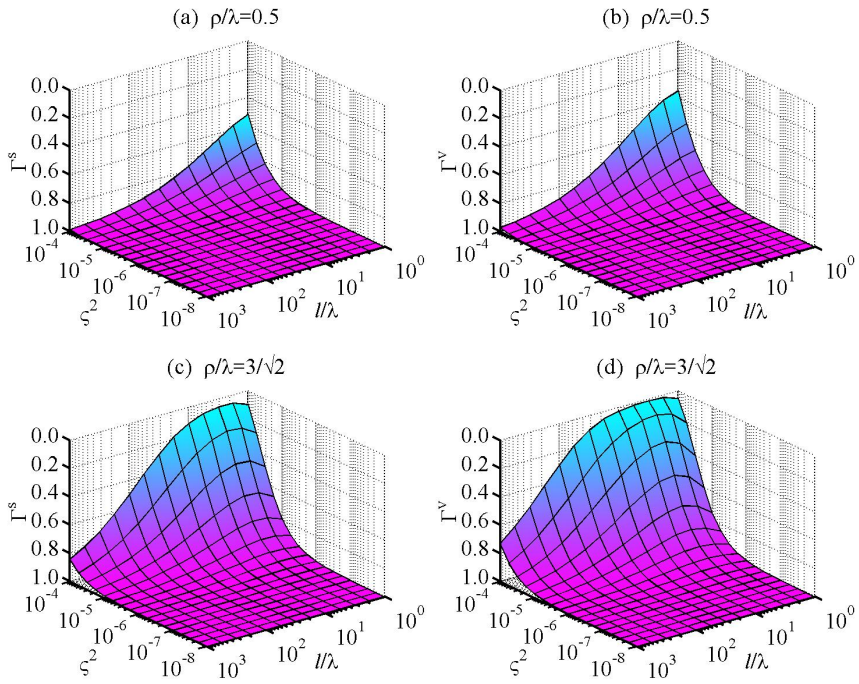

Figure 3: Coherence for an incident plane wave: (a) and (c) are for a scalar von Kármán spectrum; (b) and (d) are for a vector von Kármán spectrum. All calculations are for $r/\lambda = 500$.

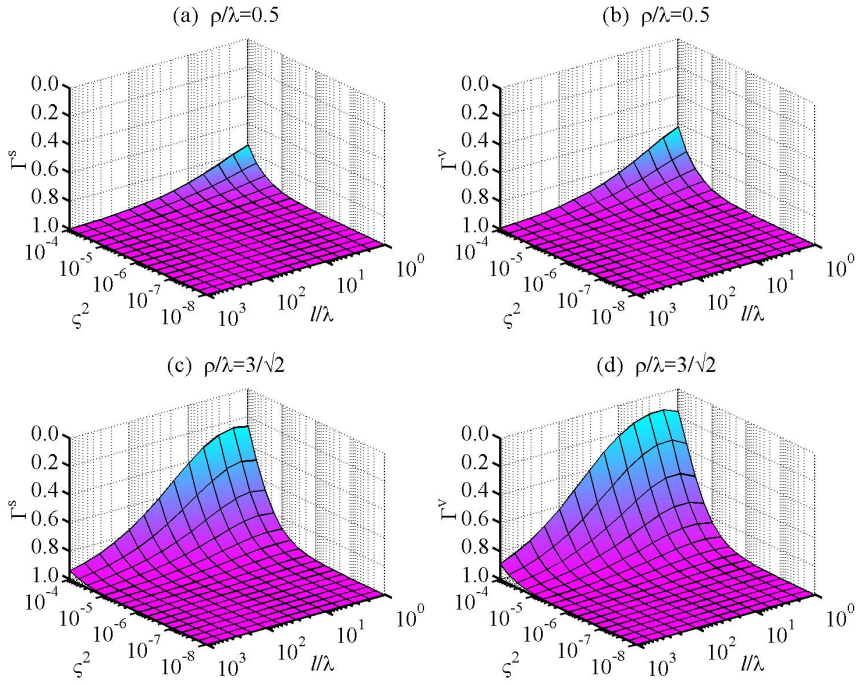

Figure 4: Coherence for an incident spherical wave: (a) and (c) are for a scalar von Kármán spectrum; (b) and (d) are for a vector von Kármán spectrum. All calculations are for $r/\lambda = 500$.

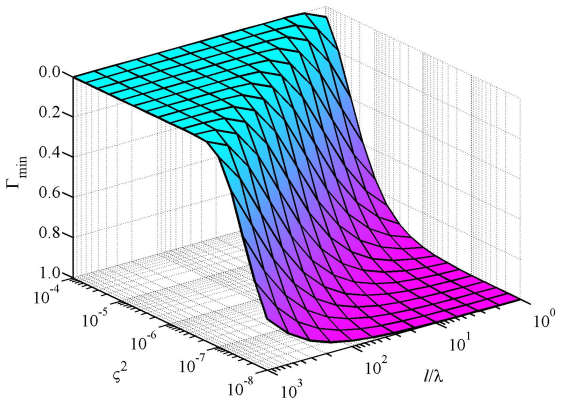

Figure 5: Minimum coherence ($\rho = \infty$) for von Kármán spectra, $\Gamma_{\min} = e^{-2\gamma r}$. Calculation is for $r/\lambda = 500$.

evident from the units involved. The minimum value of σ_ν^2 is $\sigma_{\nu_0}^2 \equiv 1/J_{\nu\nu}$, i.e., the CRLB when Θ_ν is the only unknown. As the number of unknowns increases, σ_ν^2 will increase.

For example, suppose that there are two unknowns. The FI is

$$\mathbf{J} = \begin{bmatrix} J_{11} & J_{12} \\ J_{12} & J_{22} \end{bmatrix}, \tag{41}$$

as it is symmetric for real unknown parameters. For λ and ν cyclic (i.e., if $\lambda = 1$ then $\nu = 2$, etc.)

$$\sigma_\lambda^2 = \left(J_{\lambda\lambda} - J_{\lambda\nu}^2/J_{\nu\nu}\right)^{-1} = \sigma_{\lambda_0}^2 \left(1 - \zeta_{12}\right)^{-1} \tag{42}$$

where

$$\zeta_{12} \equiv \frac{J_{12}^2}{J_{11}J_{22}} = 1 - \frac{\sigma_{1_0}^2}{\sigma_1^2} = 1 - \frac{\sigma_{2_0}^2}{\sigma_2^2}, \qquad 0 \le \zeta_{12} \le 1\,. \tag{43}$$

Only if $J_{12} = 0$ does $\sigma_\lambda^2 = \sigma_{\lambda_0}^2$, and the estimates of Θ_1 and Θ_2 are said to be uncoupled. As ζ_{12} increases, σ_λ^2 increases from its minimum value of $\sigma_{\lambda_0}^2$, and a degradation of the estimates of Θ_1 and Θ_2 results. The quantity ζ_{12} thus provides a measure of the strength of the coupling between, and hence degradation of, the estimates of Θ_1 and Θ_2: if $\zeta_{12} = 0$, the estimates are uncoupled and the CRLBs retain their minimum values; if $\zeta_{12} \ll 1$, the estimates of θ_1 and θ_2 are weakly coupled and the CRLBs increase only slightly; and if $\zeta_{12} = 1$, the estimates are fully coupled, the CRLBs are infinite, and hence neither Θ_1 nor Θ_2 can be estimated. It is therefore advantageous to determine the conditions underwhich the estimates of Θ_1 and Θ_2 will decouple. If there are more than two coupled parameter estimates, we define the coupling between the λth and νth parameter estimates to be

$$\zeta_{\lambda\nu} \equiv \frac{J_{\lambda\nu}^2}{J_{\lambda\lambda}J_{\nu\nu}}\,. \tag{44}$$

In this way, we have a measure of the coupling strength between any two given parameters.

3.2 Fisher Information of Theoretical Model

The dependence of the FI on all the unknown parameters except the signal-to-noise ratio has clearly been established. The SNR is related to the noise variance by $\mathrm{SNR} = p_0^2/\sigma_n^2$. It is often useful to express the SNR in decibels $\mathrm{SNR}_{\mathrm{dB}}$, $\mathrm{SNR} = 10^{\mathrm{SNR}_{\mathrm{dB}}/10}$. For the plane wave case, p_0 is a constant, and we treat the SNR as the unknown. In this way, the exact value of p_0 is not needed for the calculation, as the FI may be renormalized by p_0^2. For a spherical wave p_0 is dependent upon r, therefore we consider SNR_0, the signal-to-noise ratio at a distance $\mathcal{R}_0$, as the unknown. Then $\sigma_n^2 = (\mathcal{A}r_0)^2/(\mathrm{SNR}_0\mathcal{R}_0^2)$. By renormalizing the FI by $(\mathcal{A}r_0)^2$, the explicit value of $\mathcal{A}r_0$ is not needed.

The FI may be calculated from Eq. (40) for those parameters we wish to consider as unknowns: ϕ, θ, χ, r, l, ς^2, or SNR. For a deterministic mean, χ must be treated as an unknown parameter [22, 23, 24]. While the

derivatives of the covariance matrix and mean are straight forward, the derivatives with respect to turbulence parameter l are tedious. For brevity, none of the derivatives are presented here. We may interchangeably refer to the CRLB of the elevation and zenith, for as they are related by a linear transformation, their CRLBs are the same. (Linear transformations preserve the efficiency of an estimator [5].)

3.3 No Turbulence

Let us begin by examining the case of no turbulence. In the absence of turbulence

$$\boldsymbol{\mu} = p_0 \left[e^{\mathrm{i}\Phi_1},\ e^{\mathrm{i}\Phi_2},\ \ldots,\ e^{\mathrm{i}\Phi_N} \right]^{\mathrm{T}} \quad \text{and} \quad \mathbf{C} = \sigma_n^2 \mathbf{I}_N. \tag{45}$$

The elements of the FI matrix are

$$J_{\lambda\nu} = \frac{MN}{\sigma_n^4} \frac{\partial \sigma_n^2}{\partial \Theta_\lambda} \frac{\partial \sigma_n^2}{\partial \Theta_\nu} + \frac{2MN}{\sigma_n^2} \frac{\partial p_0^2}{\partial \Theta_\lambda} \frac{\partial p_0^2}{\partial \Theta_\nu} + 2M \frac{p_0^2}{\sigma_n^2} \sum_{i=1}^{N} \frac{\partial \Phi_i}{\partial \Theta_\lambda} \frac{\partial \Phi_i}{\partial \Theta_\nu}. \tag{46}$$

By setting $J_{\lambda\nu} = 0$, we may determine the conditions underwhich the estimates of Θ_λ and Θ_ν will decouple.

3.3.1 Plane Wave

Let us consider ϕ, θ, and χ as unknowns, and r and SNR as knowns. The estimate of χ will decouple from the estimates of ϕ and θ for every value of ϕ and θ if

$$\sum_{i=1}^{N} x_i' = \sum_{i=1}^{N} y_i' = \sum_{i=1}^{N} z_i' = 0, \tag{47}$$

i.e., if the center of the array is located at the origin. [If r is unknown, the estimate of r will also decouple from the estimates of ϕ and θ if Eq. (47) is satisfied.] The estimates of ϕ and θ will decouple from one another if

$$\sum_{i=1}^{N} {y_i'}^2 = \sum_{i=1}^{N} {x_i'}^2 \qquad \text{and} \qquad \sum_{i=1}^{N} x_i' y_i' = \sum_{i=1}^{N} x_i' z_i' = \sum_{i=1}^{N} y_i' z_i' = 0. \tag{48}$$

Symmetric planar array configurations such as a circular array with sensors placed at equal angular intervals, or a rectangular grid with sensors placed at the lattice points, meet these requirements provided that the array is located in the xy-plane and that the array center is located at the origin. (If both r and χ are unknown, then the quantity $\chi' = kr + \chi$ (the phase of the signal at the array center) may be treated as the unknown, and the same results hold. Nielsen [18] has performed an analysis for a multiple-frequency, far-field, sine wave signal imbedded in Gaussian noise. The conditions he found for the estimates of the elevation, azimuth, and phase at the array center to decouple are the same as for the case presented here. Among the literature which examine array configurations that result in the decoupling of the angle estimates, Refs. [19, 20, 21] may be of interest to the reader.)

Suppose that the center of a sensor array is located at the origin. Then if the sensors are configured so that Eq. (48) is satisfied,

$$\frac{1}{\sigma_\phi^2} = 2Mk^2 \cos^2\theta \frac{p_0^2}{\sigma_n^2} \sum_{i=1}^{N} {x_i'}^2 \qquad \text{and} \qquad \frac{1}{\sigma_\theta^2} = 2Mk^2 \frac{p_0^2}{\sigma_n^2} \sum_{i=1}^{N} \left({x_i'}^2 \sin^2\theta + {z_i'}^2 \cos^2\theta \right). \tag{49}$$

At $\theta = \pi/2$, the CRLB of ϕ is singular. Therefore, such array configurations cannot be used to estimate the azimuthal AOA of a wave that is propagating along the z-axis. Specifically, a planar array must be located in the xy-plane in order for Eq. (48) to be satisfied. Thus it cannot be used to estimate the azimuth of a normally incident wave. Due to the limitations of the turbulence model discussed in Sect. 2.1, we want to investigate waves that are nominally normal to a planar array. Therefore in the full simulation, the estimates of the azimuth and elevation will always be coupled as we cannot choose the xy-plane as the array plane.

3.3.2 Spherical Wave

Now let us consider a spherical wave. Suppose that r and SNR are known, and that ϕ, θ, and χ are unknown. The estimates of ϕ and θ will decouple from the estimate of χ for every value ϕ and θ if

$$\sum_{i=1}^{N} \frac{x_i'}{r_i} = \sum_{i=1}^{N} \frac{y_i'}{r_i} = \sum_{i=1}^{N} \frac{z_i'}{r_i} = 0\,. \tag{50}$$

Therefore, unlike the plane-wave case, there is no simple array geometry that will result in the decoupling of the estimates of the AOAs from the estimate of the phase angle. The conditions for the estimates of ϕ and θ to decouple are also unattainable in practice:

$$\sum_{i=1}^{N} \frac{x_i'^2}{r_i^2} = \sum_{i=1}^{N} \frac{y_i'^2}{r_i^2} = 0 \qquad \text{and} \qquad \sum_{i=1}^{N} \frac{x_i' y_i'}{r_i^2} = \sum_{i=1}^{N} \frac{x_i' z_i'}{r_i^2} = \sum_{i=1}^{N} \frac{y_i' z_i'}{r_i^2} = 0\,. \tag{51}$$

It can also be shown that if r is also unknown, its estimate is coupled to that of ϕ, θ, and χ.

3.4 Turbulence

3.4.1 Plane Wave

Let us now consider a plane wave propagating through turbulence. Unfortunately, this case does not lend itself to being evaluated analytically. We assume that the wave is propagating near the x-axis and thus take the yz-plane to be the array plane. The origin is taken to be at the center of the array. As noted earlier, the estimates of θ and ϕ are coupled for this choice. Numerically, the estimates of θ and ϕ are found to be uncoupled from the estimates of l, ς^2, and SNR. However we find, again numerically, that placing the center of the array at the origin is no longer a sufficient condition for the estimates of ϕ and θ to decouple from the estimates of r and χ: a symmetric array configuration such as a rectangular grid with mirror symmetry in y about the origin and mirror symmetry in z about the origin must be used, though the stronger condition of uniform spacing is not necessary. The results are independent of the value of χ. (This is expected as the value of the source phase should not effect the estimates of the other parameters. Close inspection of the second term of Eq. (40) reveals that its dependence in the FI should cancel.) The estimates of r, l, ς^2, and SNR are all coupled.

3.5 Spherical Wave

For the spherical-wave analysis, we again assume that the wave is propagating near the x-axis, take the array plane to be yz-plane, and take the origin to be at the array center. Numerically, we find: the estimates of ϕ, θ, r and χ are all coupled; the estimates of ϕ and θ are uncoupled from the estimates of l, ς^2, and SNR_0; and the estimates of r, l, ς^2, and SNR_0 are all coupled. Again, the results are independent of the value of χ.

4 Results

For both the plane-wave and spherical-wave analyses, the array geometry considered is a 4×4 square grid with spacing of d. In all figures, $d/\lambda = 0.5$. As the CRLB (σ) for M independent and identically distributed datasets is $1/\sqrt{M}$ times the CRLB for one dataset, all results are presented for $M = 1$.

4.1 Plane Wave

The values of σ_ϕ, σ_θ, σ_{ϕ_0}, and σ_{θ_0} are the same for normal incidence due to symmetry. In Fig. 6, σ_ϕ for normal incidence is plotted as a function of ς^2 and l/λ for $r/\lambda = 500$ and SNR = 10 dB. A vector von Kármán turbulence spectrum is used. A peak is evident in σ_ϕ at large ς^2 and small l/λ. In this region both Γ_{ij} and $\Gamma_{\min}$ are approaching their mimimum values as functions of the turbulence parameters. In fact, in the limit that Γ_{ij} and $\Gamma_{\min}$ simultaneously approach zero, $\sigma_\phi^2 \to \infty$ as $\mathbf{C} \to \sigma_n^2 \mathbf{I}_N$ and $\boldsymbol{\mu} \to 0$. For

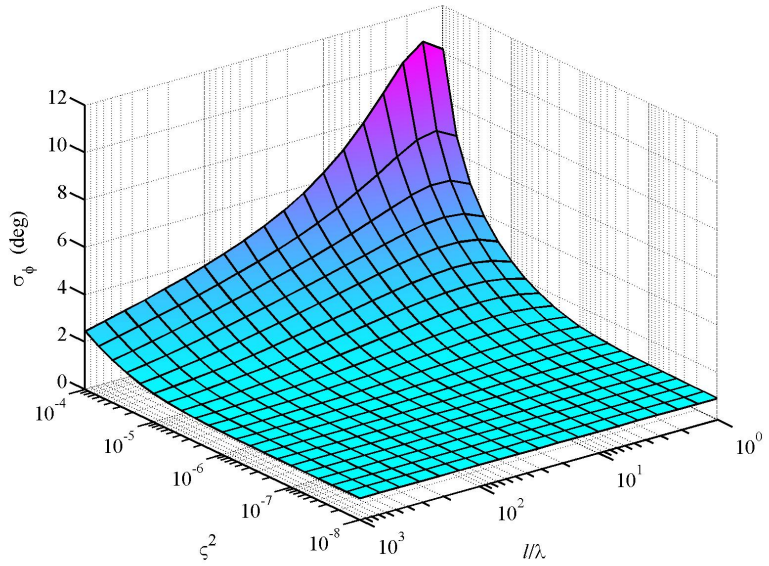

Figure 6: CRLB of ϕ for a plane wave as a function of turbulence parameters. Calculation is for normal incidence, $r/\lambda = 500$, SNR = 10 dB, and a vector von Kármán spectrum.

small values of ς^2 and l/λ, both Γ_{ij} and $\Gamma_{\min}$ are approaching the maximum value of 1.0, and hence σ_ϕ^2 is approaching the limit for no turbulence. The behavior for other values of the SNR is similar, with σ_ϕ increasing with decreasing SNR. The corresponding percent difference between σ_ϕ calculated with a zero mean and with a deterministic mean is plotted in Fig. 7. Using a deterministic mean reduces the CRLB. The largest percent difference occurs for large ς^2 and small l/λ. In this region, however, the CRLB is large and the AOAs cannot be estimated accurately. In the regions where $\Gamma_{\min} \approx 1$, the percent difference is small, though nonzero. In the regions where $\Gamma_{\min} \approx 0$, the percent difference is zero, as it should be.

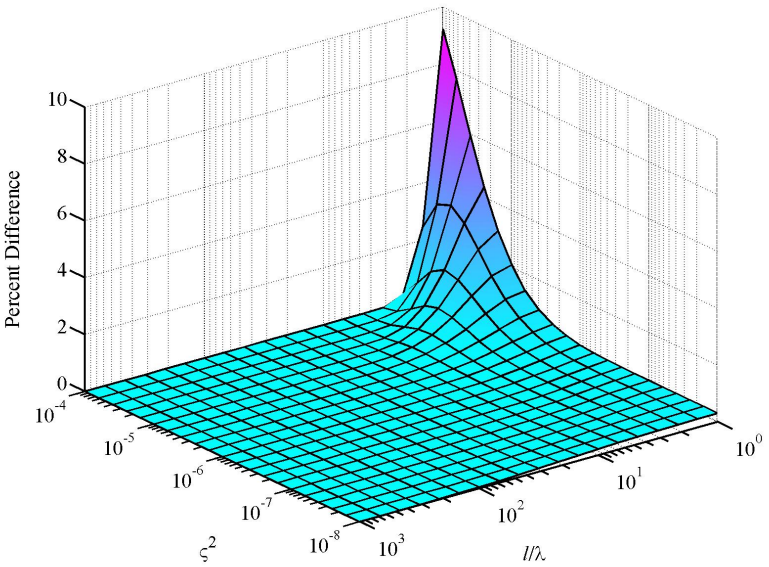

Figure 7: Percent difference of σ_ϕ for a plane wave calculated with a zero mean and with a deterministic mean. Calculation is for normal incidence, $r/\lambda = 500$, SNR = 10 dB, and a vector von Kármán spectrum.

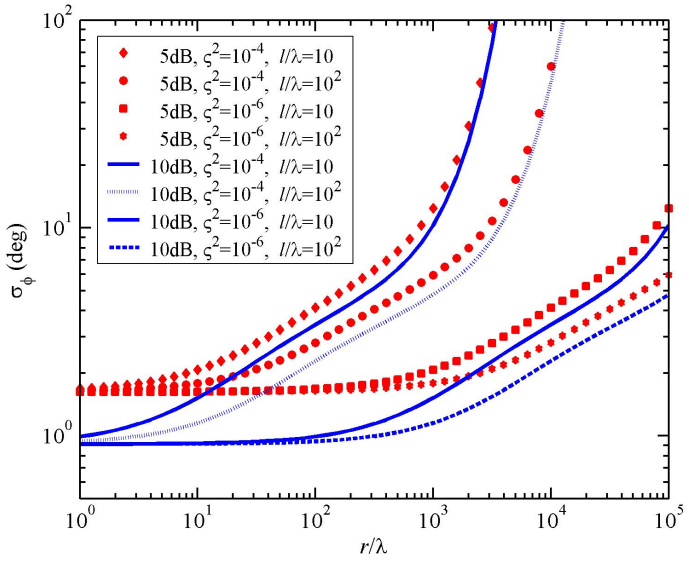

Figure 8: CRLB of ϕ for a plane wave as a function of normalized propagation distance. All curves are for normal incidence and a vector von Kármán spectrum.

In Fig. 8, σ_ϕ for normal incidence is examined as a function of the normalized propagation distance r/λ for a couple of values of the SNR, ς^2, and l/λ. A vector von Kármán spectrum is used. The points (lines) correspond to a SNR of 5 dB (10 dB) for every value of r/λ. Though the graph extends to smaller values of r/λ than are valid for the turbulence model, it is useful to see the limiting behavior of our model. [Recall the limits given in Sects. 2.1–2.2. In particular, the approximations in Eqs. (13, 14, 18–20) must hold.] For $\varsigma^2 = 10^{-6}$ and $r/\lambda \lesssim 400$, σ_ϕ is limited by the SNR. As r/λ increases, σ_ϕ is driven primarly by the values of the turbulence parameters, in particular, the index-of-refraction variance. The corresponding percent difference of σ_ϕ calculated with a zero mean and with a deterministic mean is shown in Fig. 9.

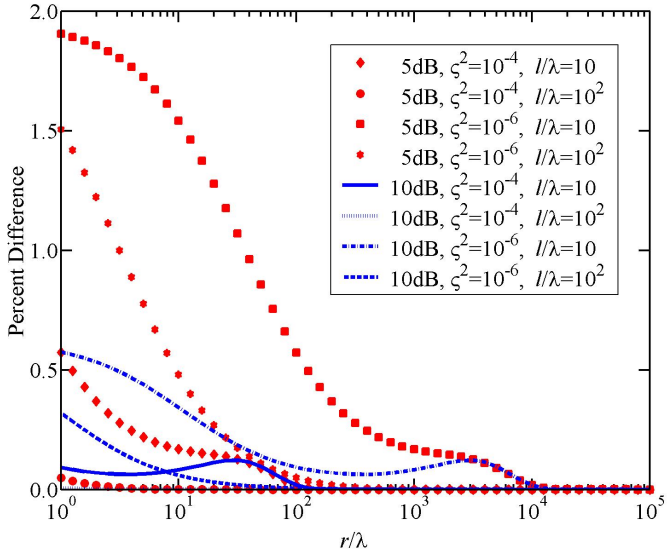

Figure 9: Percent difference of σ_ϕ for a plane wave calculated with a zero mean and with a deterministic mean as a function of normalized propagation distance. All curves are for normal incidence and a vector von Kármán spectrum.

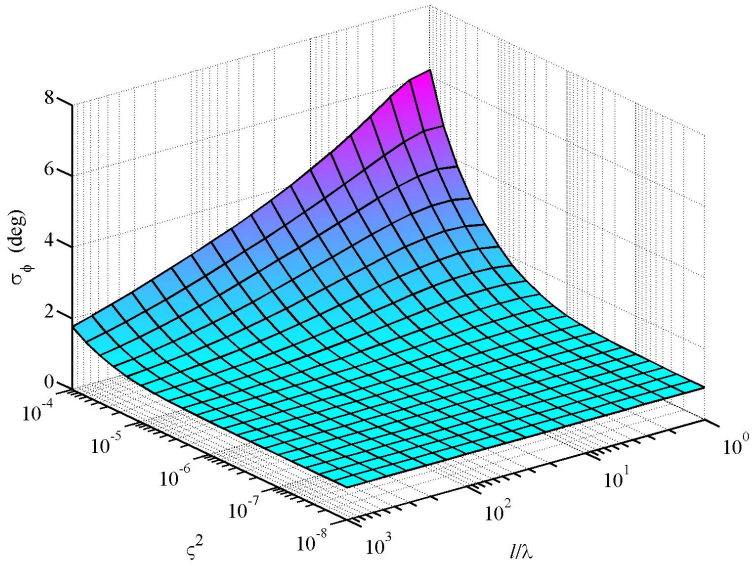

Figure 10: CRLB of ϕ for a spherical wave as a function of turbulence parameters. Calculation is for normal incidence, $r/\lambda = 500$, $\mathrm{SNR}_0 = 10\,\mathrm{dB}$ at $\mathcal{R}_0/\lambda = 500$, and a vector von Kármán spectrum.

All plots presented have been for normal incidence. The results for other values of ϕ and θ are similar. As ϕ and θ increase, σ_ϕ and σ_θ increase. The angular dependence of σ_ϕ and σ_θ is discussed in Refs. [22, 23] for the same array geometry that is considered here. Of particular interest is the coupling $\zeta_{\phi\theta}$. In Refs. [22, 23], $\zeta_{\phi\theta}$ is found to be the same as for the no turbulence case:

$$\zeta_{\phi\theta} = \frac{\sin^2\phi\sin^2\theta}{\cos^2\theta + \sin^2\phi\sin^2\theta} \approx \phi^2\theta^2 - \frac{1}{3}\phi^4\theta^2 + \frac{2}{3}\phi^2\theta^4\,, \tag{52}$$

regardless of the the value of r/λ, d/λ, SNR, l/λ, or ς^2, and regardless of the von Kármán spectrum used. The coupling is weak: for $\phi,\ \theta \le 15^\circ$, $\zeta_{\phi\theta} \sim 10^{-3}$.

A vector von Kármán spectrum was considered in Figs. 6–9. The analogous results using a scalar von Kármán spectrum are similar. As a function of turbulence parameters, the shape of the curves are nearly identical, but the value of σ_ϕ is for the most part smaller. The largest difference occurs in the regions where the MCF for the scalar spectrum is appreciably larger than the MCF for a vector spectrum (refer back to Fig. 3). More details of the results for a scalar spectrum are given in Refs. [22, 23]. The percent difference of σ_ϕ using a zeromean and a deterministic mean is also smaller; in particular, the peak at large ς^2 and small l/λ is reduced. Again, the use of a deterministic mean reduces the CRLB.

4.2 Spherical Wave

As we are assuming spherical propagation of the wave, the signal-to-noise ratio is now dependent upon r. Recall that the signal-to-noise ratio evaluated at $r = \mathcal{R}_0$ is denoted SNR_0.

Again, the values of σ_ϕ, σ_θ, $\sigma_{\phi 0}$, and $\sigma_{\theta 0}$ are the same at for normal incidence due symmetry. In Fig. 10, σ_ϕ for normal incidence is plotted versus l/λ and ς^2 for $r/\lambda = 500$ and $\mathrm{SNR}_0 = 10$ dB at $\mathcal{R}_0/\lambda = 500$. A vector von Kármán spectrum is used. The overall values of σ_ϕ are smaller than for the plane-wave case. This is expected as the values of the MCF for a plane wave are smaller than for a spherical (refer back to Figs. 3–4). The corresponding percent difference of σ_ϕ calculated with a zero mean and with a deterministic mean is given in Fig. 11. As with the plane wave case, the use of a deterministic mean reduces the CRLBs of the AOAs. The results are similar for other values of the SNR.

In Fig. 12, σ_ϕ for normal incidence is plotted versus the normalized propagation distance. Two values of

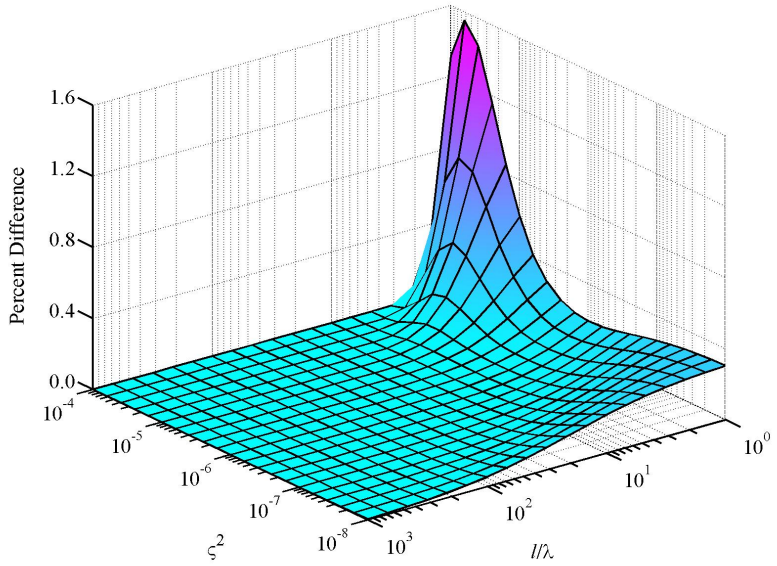

Figure 11: Percent difference of σ_ϕ for a spherical wave calculated with zero mean and with a deterministic mean as a function of turbulence parameters. Calculation is for normal incidence, $r/\lambda = 500$, $\mathrm{SNR}_0 = 10\,\mathrm{dB}$ at $\mathcal{R}_0/\lambda = 500$, and a vector von Kármán spectrum.

ς^2, l/λ, and SNR_0 evaluated at $\mathcal{R}_0/\lambda = 500$ are considered. A vector von Kármán spectrum is used. Again, the graph is extended to include smaller values of r/λ than are valid for the turbulence model. At small values of r/λ, we see that σ_ϕ is dependent upon the values of the turbulence parameters (particularly ς^2) and is independent of the value of SNR_0. Note the difference between the outward spherical propagation and the plane wave propagation depicted in Fig. 8. The corresponding percent difference of σ_ϕ calculated with a zero mean and with a deterministic mean is given in Fig. 13.

Again, only the results for normal incidence have been shown. For other values of ϕ and θ, the results are similiar and σ_ϕ and σ_θ increase with increasing ϕ and θ. At $\phi = \theta = 0$, the coupling between the estimates of ϕ and θ and the estimates of r and χ is zero. At $r/\lambda = 500$ and $l/\lambda = 10$, we find that for $\phi,\ \theta \leq 15°$: $\zeta_{\phi\, r/\lambda}$ and $\zeta_{\theta\, r/\lambda}$ are on the order of 10^{-9} for $\varsigma^2 = 10^{-6}$, and on the order of 10^{-11} for $\varsigma^2 = 10^{-4}$; $\zeta_{\phi\chi}$ and $\zeta_{\theta\chi}$ are on the order of 10^{-9} for $\varsigma^2 = 10^{-6}$, and on the order of 10^{-20} for $\varsigma^2 = 10^{-4}$; and $\zeta_{\phi\theta}$ is on the order of 10^{-3}. Therefore, the coupling between the estimates of ϕ and θ and estimates of χ and r/λ are negigible for these cases. Moreover, as r/λ increases, these couplings rapidly approach zero. Reference [24] addresses the angular dependence and couplings in more detail.

As with the plane wave case, the results for a scalar von Kármán spectrum are very similar to those for a vector spectrum. The CRLBs of the AOAs are smaller for a scalar spectrum. The use of a deterministic mean reduces the CRLBs of the AOAs, though percent difference is not as pronounced as for the vector spectrum.

5 Conclusions

The performance bounds of acoustic arrays operating in atmospheric turbulence with fluctuations described by a von Kármán spectrum have been examined. This analysis features four main improvements upon earlier work: (1) The performance bounds have been generalized to weak as well as strong scattering. (2) Multiple unknowns such as the propagation distance of the wavefront, turbulence parameters, phase of the source, and signal-to-noise ratio have been incorporated. (3) AOA estimates for three-dimensional problems (i.e., two bearing angles) have been considered. (4) A multivariate analysis for an incident spherical

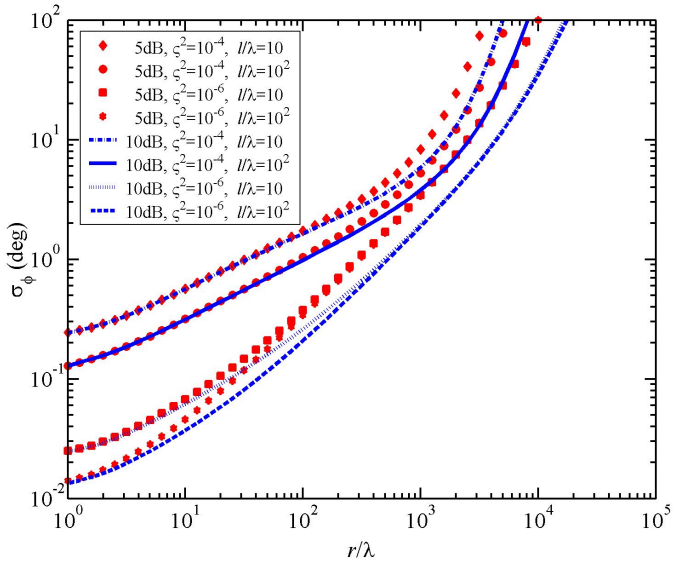

Figure 12: CRLB of ϕ for a spherical wave as a function of normalized propagation distance. Calculation is for normal incidence, SNR_0 evaluated at $\mathcal{R}_0/\lambda = 500$, and a vector von Kármán spectrum.

wave has been developed in addition to that for an incident plane wave.

The primary interest was to analyze the Cramer-Rao lower bounds of the angles of arrival. For an incident plane wave, we have found that an appropriate choice of coordinate system and array geometry leads to the decoupling of the estimates of the AOAs from the estimates of the other parameters: the normalized propagation distance (r/λ), SNR, turbulence parameters (l/λ and ς^2), and phase angle of the source (χ). In order to remain consistent with the small-angle approximation, we had to choose a coordinate system that

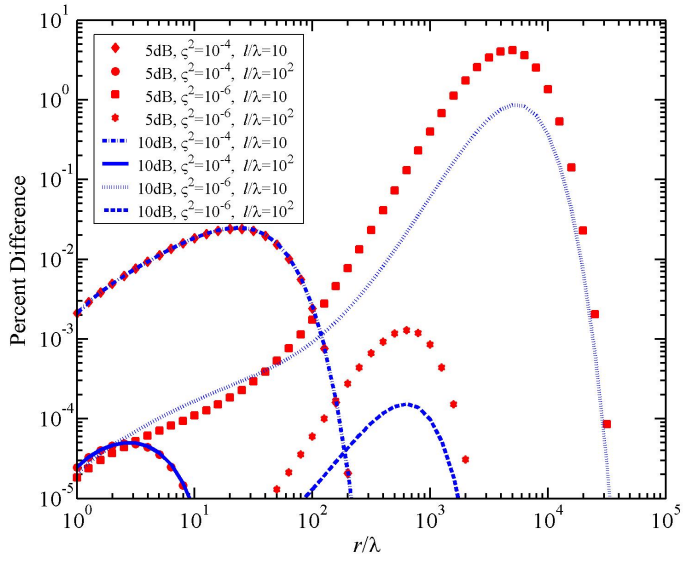

Figure 13: Percent difference of σ_ϕ for a spherical wave calculated with a zero mean and with a deterministic mean as a function of normalized propagation distance. Calculation is for normal incidence, SNR_0 evaluated at $\mathcal{R}_0/\lambda = 500$, and a vector von Kármán spectrum.

resulted in the coupling of the estimates of the azimuth and zenith; the coupling, however, was small. For large values of the index-of-refraction variance and moderate to small values of the normalized length scale, we have found that the CRLBs of the AOAs increase significantly at large propagation distances. However, for smaller values of the index-of-refraction variance and normalized propagation distance, the SNR is the limiting factor.

For an incident spherical wave, we have found that the estimates of the AOAs are coupled to the estimates of the normalized propagation distance, the phase angle of the source, and to one another. The estimates of the AOAs are uncoupled from the estimates of the turbulence parameters and SNR_0. For the array geometry considered, the couplings between the estimates of the AOAs and the estimates of source phase and normalized propagation distance are negigible, and the coupling of the estimates of the azimuth and elevation is weak. For small values of the normalized propagation distance, the CRLBs of the AOAs are dependent upon turbulence parameters and independent of SNR_0.

We have found that for both a plane wave and a spherical wave, the use of a deterministic mean reduces the CRLBs of the AOAs from that calculated with a zero mean. The effect is more prevelant for a vector von Kármán spectrum than for a scalar. However, the largest percent difference occurs in the regions where the CRLBs are large, and hence the AOAs cannot be well estimated. Therefore, for this analysis the inclusion of a deterministic mean is not very significant. However, for other models of the MCF, the percent difference may be more significant, and thus a deterministic mean should be considered.

The results of this analysis demonstrate that scattering by atmospheric turbulence significantly affects the performance of acoustic sensor arrays. In order to understand and circumvent limitations on Army acoustical tracking systems, it is necessary to predict the performance of acoustic sensor arrays for various atmospheric conditions. This analysis clearly demonstrates the atmospheric conditions that are unfavorable for accurate acoustical tracking. While only a single array with a simple geometry was considered in this analysis, the results indicate that the effects of atmospheric turbulence should be included in performance bounds calculations for other more complicated systems as well.

This analysis would benefit from an improved model of the second moment for oblique incidence. Future efforts should attempt to incorporate the additional phenomena of ground reflections and refraction by atmospheric wind and temperature gradients. These phenomena will likely have a considerable impact on the ability to estimate the elevation. Numerical techniques will be required to model these effects.

Acknowledgments

S. L. Collier was supported by an American Society for Engineering Education postdoctoral fellowship during the completion of the majority of this work. The authors are grateful to B. M. Sadler and A. Swami of ARL and to V. E. Ostashev of NOAA/Environmental Technology Laboratory for many helpful discussions.

References

[1] D. K. Wilson, C. R. Tate, D. C. Swanson, and D. M. Reichard, "Acoustic scintillations and angle-of-arrival fluctuations observed outdoors with a large planar vertical michrophone array," Acoustics Research Letters Online, **106**, L24-L29 (1999).

[2] B. G. Ferguson, "Variability in the passive ranging of acoustic sources in air using a wavefront curvature technique," J. Acoust. Soc. Am. **108**, 1535–1544 (2000).

[3] B. J. Uscinski and D. E. Reeve, "The effect of ocean inhomogeneities on array output," J. Acoust. Soc. Am. **87**, 2527–2534 (1990).

[4] E. Y. Gorodetskaya, A. I. Malekhanov, A. G. Sazontov, and N. K. Vdovicheva, "Deep-water acoustic coherence at long ranges: Theoretical prediction and effects on large-array signal processing," IEEE J. Ocean. Eng. **24**, 156–171 (1999).

[5] Steven M. Kay, *Fundamentals of Statistical Signal Processing: Estimation Theory* (PTR Prentice Hall, Englewood Cliffs, NJ, 1993).

[6] Louis L. Scharf, *Statistical Signal Process: Detection, Estimation, and Time Series Analysis* (Addison-Wesley, Reading, MA, 1991).

[7] B. Ottersten, M. Viberg, P. Stoica, and A. Nehorai, "Exact and large sample maximum likelihood techniques for parameter estimation and detection in array processing," J. Acoust. Soc. Am. **99**, 1370-1379 (1996).

[8] Bong-Gee Song and James A. Ritcey, "Angle of arrival estimation of plane waves propagating in random media," J. Acoust. Soc. Am. **99**, 1370-1379 (1996).

[9] D. Keith Wilson, "Performance bounds for acoustic direction-of-arrival arrays operating in atmospheric turbulence," J. Acoust. Soc. Am. **103**, 1306-1319 (1998).

[10] Vladimir E. Ostashev, *Acoustics in Moving Inhomogeneous Media* (E & FN Spon, London, 1997).

[11] J. R. Garratt, *The Atmospheric Boundary Layer* (Cambridge University Press, New York, 1992).

[12] Stanley M. Flatte, *Sound Transmission through the Fluctuating Ocean* (Cambridge University Press, New York, 1979).

[13] Akira Ishimaru, *Wave Propagation and Scattering in Random Media* (IEEE Press, Piscataway, NJ, 1997).

[14] S. M. Rytov, Yu. A. Kravtsov, and V. I. Tatarskii, *Principles of Statistical Radiophysics 4: Wave Propagation Through Random Media* (Springer-Verlag, New York, 1989).

[15] D. Keith Wilson, "Atmospheric Effects on Acoustic Arrays: A Broad Perspective From Models," IRIS Symposium on Battlefield Acoustics and Seismics, Laurel, MD (1999).

[16] V. E. Ostashev and D. K. Wilson, "Relative Contributions from Temperature and Wind Velocity Fluctuations to the Statistical Moments of a Sound Field in a Turbulent Atmosphere," Acustica **86**, 260-268 (2000).

[17] D. Keith Wilson, "A turbulence spectral model for sound propagation in the atmosphere that incorporates shear and buoyancy forcings," J. Acoust. Soc. Am. **108**, 2021-2038 (2000).

[18] Richard O. Nielsen, "Estimation of Azimuth and Elevation Angles for a Plane Wave Sine Wave with a 3-D Array," IEEE Trans. Sig. Proc. **42**, 3274-3276 (1994).

[19] Richard O. Nielsen, "Azimuth and Elevation Angle Estimation with a Three-Dimensional Array," IEEE J. Ocean Engineering **19**, 84-86 (1994).

[20] Adam N. Mirkin and Leon H. Sibul, "Cramer-Rao Bounds on Angle Estimation with a Two-Dimensional Array," IEEE Trans. Sig. Proc. **39**, 515-517 (1991).

[21] Yingbo Hua and Tapan K. Sarkar, "A Note on the Cramer-Rao Bound for 2-D Direction Finding Based on 2-D Array," IEEE Trans. on Sig. Proc. **39**, 1215-1218 (1991).

[22] S. L. Collier and D. K. Wilson, "Performance Bounds on Atmospheric Acoustic Sensor Arrays Operating in a Turbulent Medium. I. Plane-Wave Analysis," U. S. Army Research Laboratory, ARL-TR-2426.

[23] S. L. Collier and D. K. Wilson, "Performance Bounds for Passive Sensor Arrays Operating in a Turbulent Medium: Plane-Wave Analysis," submitted to J. Acoust. Soc. Am.

[24] S. L. Collier and D. K. Wilson, "Performance Bounds for Passive Sensor Arrays Operating in a Turbulent Medium: II. Spherical-Wave Analysis," in preparation for submission to J. Acoust. Soc. Am.